Supporting Information

Fernandez-Marcos et al. 10.1073/pnas.0813055106

SI Materials and Methods

Reagents. IKK inhibitors PS1145 and BMS-345541 were from Sigma.

Histological Analysis. Sections were deparaffinized, rehydrated, and treated for antigen retrieval. After quenching of endogenous peroxidase and blocking in normal serum, tissues were incubated with primary antibody overnight at 4 °C, followed by incubation with biotinylated secondary antibody. Antibodies were visualized with avidin-biotin complex (Vectastain Elite, Vector Labs) using diaminobenzidine as the chromagen. Slides were then counterstained with hematoxylin, dehydrated, and mounted. For IHC, the following antibodies were used: Par-4 (R-334), p65 (C-20), and synaptophysin (D-4) from Santa Cruz; pAkt-S473 (4058), pp65-S276 (3037), and pIKK-S176/180 (2697) from Cell Signaling; laminin (L9393) from Sigma; Ki67 (sp6) and AR (Ab2) from Neomarkers; E-cadherin from Becton Dickinson; PTEN (ab31392) from Abcam; anti-IL-6 from R&D systems; and active caspase-3 (C92–605) from BD-PharMingen. All antibodies were used according to manufacturers' instructions. Quantification of positive nuclear staining was determined by counting 10 fields for each condition at 40× magnification.

For IHC analysis of human samples, a series of prostate carcinomas ($n = 41$) obtained from surgical specimens from University Hospital "La Paz" Madrid was used. IHC was done on human tissue microarray sections. Representative areas of tumors ($n = 37$) were carefully selected on H&E-stained sections and marked on individual paraffin blocks. Two-millimeter-diameter tissue cores were obtained from each specimen. The tissue cores were precisely arrayed in a paraffin block using a tissue microarray workstation (Beecher Instruments). The tissue microarray included normal adjacent tissue for each tumor sample to evaluate variations in tissue fixation between samples. An H&E-stained section was reviewed to confirm the presence of morphologically representative areas of the original lesions. The IHC analysis was done using the following antibodies: antiPar-4 (Abcam) and PTEN (Cell Signaling).

Histopathological analysis of mouse samples were performed by E.A.C. and M. Canamero PIN was categorized into 4 different grades according to Park et al. (1): PIN I, containing small foci with 1 or 2 layers of atypical cells; PIN II, with 2 or more layers of atypical cells that do not fill the lumen; PIN III, with normal duct outlines, but with the lumen filled by cells with large and pleomorphic nuclei; and PIN IV, with the lumen filled with atypical cells and distorted and irregular duct profiles with central necrosis and host inflammatory responses.

***Par-4* Promoter Hypermethylation Analysis.** Methylation-specific PCR was performed as described elsewhere (2).

Cell Culture. WT and Par-4$^{-/-}$ primary EFs were derived from E13.5 embryos (3). Cells were maintained in DMEM (Gibco BRL) supplemented with 10% (vol/vol) FCS (FCS), 1% glutamine, and 1% penicillin/streptomycin (Gibco-Invitrogen) in 5% CO_2, and immortalized by retroviral infection with pBabeT-Ag followed by puromycin selection (1 mg/ml). The established cell lines represent pools of at least 100 independent clones. The PTEN CaP2 cell line, a generous gift from H. Wu, was maintained as previously described (4). Knockdown cell lines for Par-4 and PTEN were generated by infection with lentivirus. Par-4 and PTEN lentiviruses were from OpenBiosystems. Lentivirus stocks were produced by the Viral Vector Core at the Translational Core Laboratories, Cincinnati Children's Hospital Research Foundation (Cincinnati, Ohio). Mouse IKKβ and AKT sRNAi were from Qiagen.

Measurements of Apoptosis. Apoptotic cells were detected in histological preparations using the TUNEL Apop Tag peroxidase in situ apoptosis detection kit (Chemicon) following the the manufacturer's instructions and counting positive cells under the microscope; alternatively, when indicated, apoptosis was measured by staining for active caspase-3 and quantifying using a Dotslide scanner (Olympus) with the Olyvia software.

Western Blot. Cell extracts were prepared for Western blot in RIPA buffer (1× PBS, 1% Nonidet P-40, 0.5% sodium deoxycholate, 0.1% SDS, 1 mM phenyl methyl sulfonyl fluoride and protease inhibitors). Lysates were separated by SDS/PAGE and transferred to Nitrocellulose-ECL membranes (GE Healthcare) and the immune-complex was detected by chemiluminescence (GE Healthcare). The following antibodies were used for Western blot analyses: PTEN (A2B1), Par-4 (R-334), p65 (C-20), IKKα/βH744, actin (I-19), and secondary antibodies from Santa Cruz; and pAkt-S473 (4058), Akt (9272), pp65-S536 (3033), pp65-S276 (3037), pIkB (2859), IkB (4812), pIKK-S176/180 (2697), pStat3-Y705 (9138) and pStat3-S727 (9136) from Cell Signaling. All antibodies were used according to manufacturers' instructions.

Soft-Agar Assays. To determine the ability of cells to grow in soft agar, 2×10^4 cells were suspended in 0.3% agar in DMEM plus 10% FCS and overlaid on 0.5% agar in the same medium. Cells were re-fed with 10% FCS-containing medium every 5 days.

Confocal Analysis. EFs were fixed with 4% formaldehyde and permeabilized with 0.1% Triton X-100. Free aldehyde groups were quenched with 50 mM NH4Cl. Endogenous peroxidase activity was quenched by treatment with 3% H_2O_2 in methanol for 15 min. Fixed cells were blocked in blocking solution. Cells were incubated with anti-p65 for 1 h at 37 °C and followed by the Tyramide-Alexa 488 system (Molecular Probes). Propidium iodide staining was used to detect nuclei. Glass cover slips were mounted on Mowiol and examined with a Zeiss LSM 510 Meta confocal system. Quantification of positive p65 nuclear staining was determined by counting 20 fields for each condition at 40× magnification.

Gene-Expression Analysis by qRT-PCR. Total RNA was extracted using the RNeasy purification kit (Qiagen) and DNase treated (RQ1 DNase free, Promega). cDNA was then prepared from total RNA using random primers (Promega) and the Omniscript RT kit (Qiagen). Relative levels of mRNA were determined by real-time quantitative PCR using an Eppendorf Realplex Mastercycler (Eppendorf) and the Quantitect SYBR Green PCR kit (Qiagen); 18S mRNA levels were used for normalization. Primer sequences used are as follows:

Fhc: TCGTCGTTCCGCCGCTCCA and AGCCACATCATCTCGGTCAAAA

IL-6: TTCCATCCAGTTGCCTTCTTGG and TTCTCATTTCCACGATTTCCCAG

Kc: TGTGGGAGGCTGTGTTTGTA and CGAGACGAGACCAGGAGAA

TNFα:TGTCTACTCCCAGGTTCTCTandGGGGCAGGGGCTCTTGAC

18S: GTAACCCGTTGAACCCCATT and CCATCCAATCGGTAGTAGCG

1. Park JH, et al. (2002) Prostatic intraepithelial neoplasia in genetically engineered mice. *Am J Pathol* 161(2):727–735.
2. Moreno-Bueno G, et al. (2007) Inactivation of the candidate tumor suppressor par-4 in endometrial cancer. *Cancer Res* 67(5):1927–1934.
3. Garcia-Cao I, et al. (2003) Genetic inactivation of Par4 results in hyperactivation of NF-kB and impairment of JNK and p38. *EMBO Rep* 4:307–312.
4. Jiao J, et al. (2007) Murine cell lines derived from Pten null prostate cancer show the critical role of PTEN in hormone refractory prostate cancer development. *Cancer Res* 67(13):6083–6091.

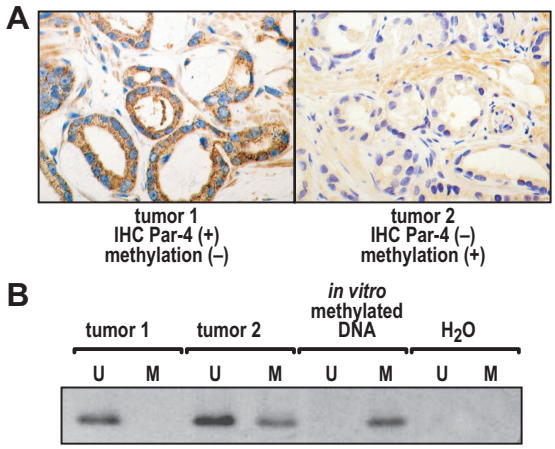

Fig. S1. Par-4 loss-of-function by promoter methylation and the association between Par-4 and PTEN expression in human prostate cancer. (*A*) Immunohistochemistry (IHC) of Par-4 in the same tumors shown in *B*. (Magnification: 40×.) Tumor 1 shows cytoplasmic Par-4, whereas tumor 2 lacks detectable Par-4. Par-4 promoter methylation was assayed by methylation-specific PCR (MSP) in primary human prostate cancers (see Tables S2 and S3). (*B*) Example of MSP analysis of 2 tumors. Tumor 1 is positive for unmethylated (U) promoter but negative for methylation (M), whereas tumor 2 contains methylated Par-4 promoter.

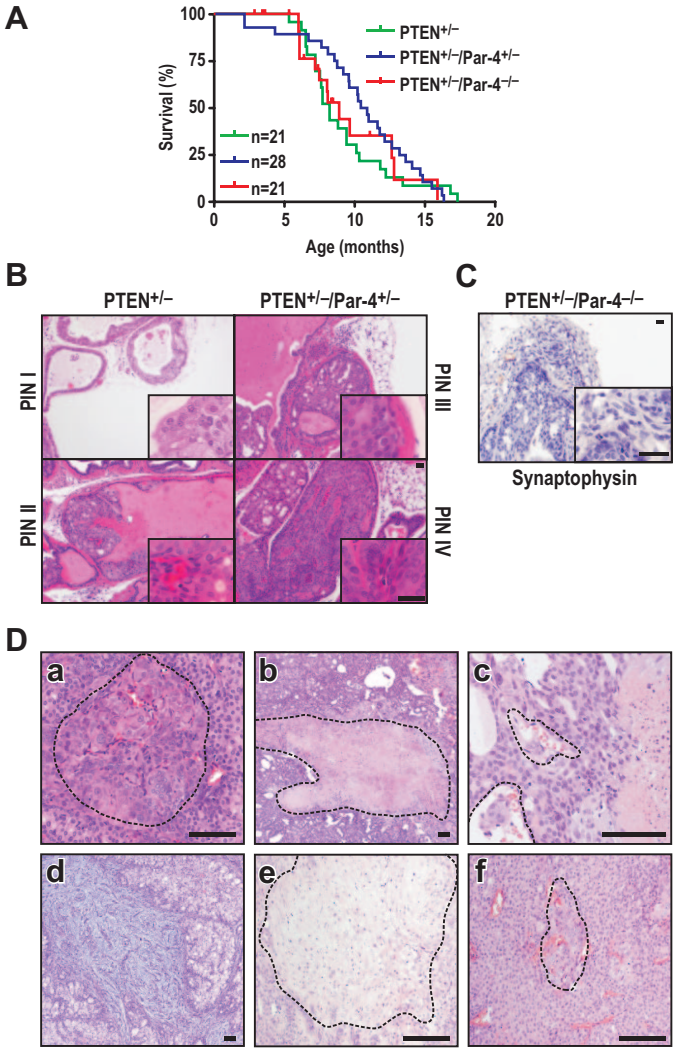

Fig. S2. Par-4$^{+/-}$ cooperates with PTEN$^{+/-}$ in the induction of invasive prostate carcinoma. (*A*) Kaplan-Meier survival curves of mice of the indicated genotypes. Mortality of these mice is mainly a result of lymphoproliferative disorders driven by PTEN-heterozygosity. Par-4 status does not affect PTEN-driven lymphoproliferation. (*B*) Representative sections of H&E staining of prostate lesions from 6-month-old mice of different genotypes. High grade PIN (PIN III and IV) is present at this age only in prostates from PTEN$^{+/-}$/Par-4$^{+/-}$ mice. (Scale bar, 50 μm.) (*C*) Staining for synaptophysin is negative in the invasive carcinoma of *PTEN*$^{+/-}$*/Par-4*$^{-/-}$ mice. (Scale bar, 50 μm.) (*D*) Characteristic histological findings in high-grade prostate carcinoma in *PTEN*$^{+/-}$*/Par-4*$^{-/-}$ mice: (*a*) focus of anaplastic cells, (*b*) large sheet of necrosis, (*c*) vascular embolus, (*d*) mixoid pattern, (*e*) fibrotic bundles, (*f*) solid growth around a focus of anaplastic cells. (Scale bar, 50 μm.)

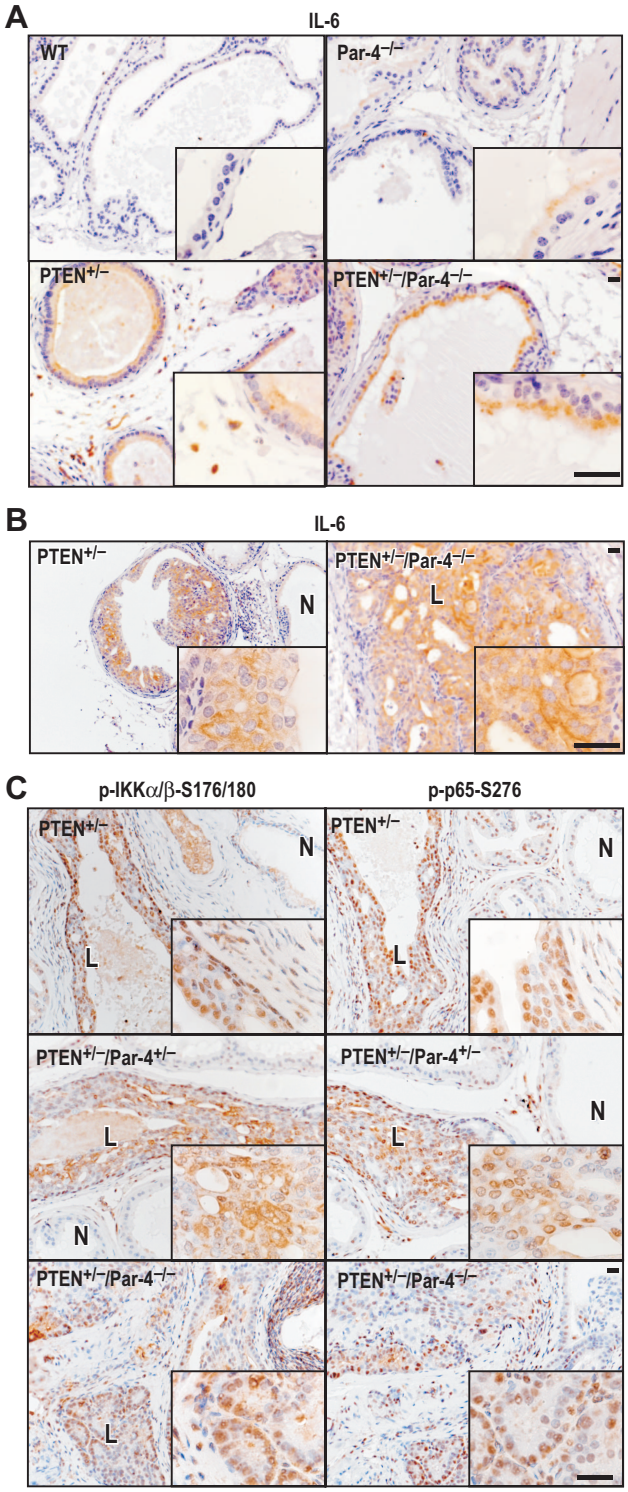

Fig. S3. IL-6 expression is enhanced in PTEN$^{+/-}$/Par-4$^{-/-}$ preneoplastic prostates. (*A* and *B*) Staining of IL-6 in preneoplastic (*A*) or PIN (*B*) prostate sections of mice of different genotypes. (*C*) Prostate sections of different genotypes were stained with anti phospho-IKKα/β (S176/180) or anti-phospho-p65 (S276). NF-κB activation is increased in PIN areas. No changes were observed between different genotypes. N, normal glands; L, lesion corresponding to PIN areas. (Scale bar, 50 μm.)

Table S1. NF-κB expression in Par-4$^{-/-}$ prostates

	WT	Par-4$^{-/-}$	Fold-change
Fhc	0.97 ± 0.48	7.49 ± 3.91*	7.72
Pecam-1	2.72 ± 1.27	10.1 ± 5.21*	3.71
Kc	4.16 ± 2.32	12.6 ± 3.30*	3.02
Xiap	0.90 ± 0.26	2.26 ± 0.95*	2.51
IL-6	2.87 ± 0.45	4.86 ± 1.51*	1.69

*, $P < 0.05$ versus WT. Values are expressed as mean ± SD.

Table S2. Par-4 expression and *PAR-4* promoter hypermethylation

Par-4 expression ($n = 41$)	n (%)
Negative/low	24 (59)
Positive	17 (41)
PAR-4 promoter hypermethylation ($n = 39$)	
Unmethylated	31 (80)
Methylated	8 (21)

Table S3. Association between Par-4 expression and *PAR-4* promoter hypermethylation

	Par-4		
	Negative/low *n* (%)	Positive *n* (%)	*P*-value
PAR-4 promoter hypermethylation ($n = 34$)			
Unmethylated	19.7 ± 0.7	11.1 ± 0.7	61.4 ± 0.8
Methylated	18.3 ± 1.1	10.2 ± 0.8	61.9 ± 1.4